Zigzag microchannel for rigid inertial separation and enrichment (Z-RISE) of cells and particles

Sajad Razavi Bazaz[1,2], Asma Mihandust[1], Robert Salomon[2,3], Hossein Ahmadi Nejad Joushani[1], Wenyan Li[3], Hoseyn A Amiri[4,5], Fateme Mirakhorli[1], Sareh Zhand[1,2], Jesus Shrestha[1], Morteza Miansari[4,5], Benjamin Thierry[6,7], Dayong Jin[2], Majid Ebrahimi Warkiani[1,2*]

[1]School of Biomedical Engineering, University of Technology Sydney, Sydney, NSW 2007, Australia

[2]Institute for Biomedical Materials & Devices (IBMD), Faculty of Science, University of Technology Sydney, Sydney, NSW 2007, Australia

[3]Children's Cancer Institute, Lowy Cancer Centre, UNSW Sydney, Kensington, NSW, Australia.

[4]Micro+Nanosystems & Applied Biophysics Laboratory, Department of Mechanical Engineering, Babol Noshirvani University of Technology, P.O. Box 484, Babol 47148-71167, Iran

[5]Department of Cancer Medicine, Cell Science Research Center, Royan Institute for Stem Cell Biology and Technology, Isar 11, Babol 47138-18983, Iran
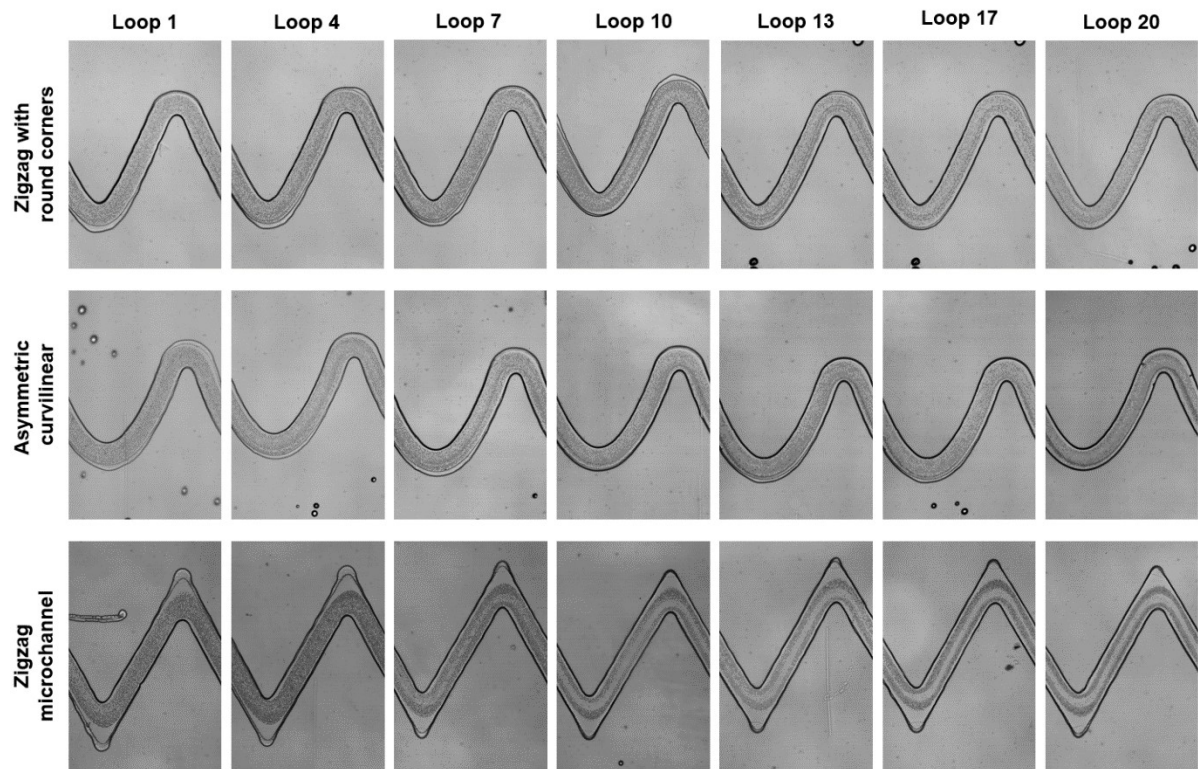
[6]Future Industries Institute, University of South Australia, Mawson Lakes Campus, Adelaide, SA, 5095 Australia

[7]ARC Centre of Excellence in Convergent Bio-Nano Science and Technology, Parkville, Victoria, 3052 Australia

The detailed description of sections listed below is provided in this part.

Table S1. Summary of confinement ratio for 3 µm to 20 µm particles in varying hydraulic diameter

Particle diameter (µm)	Hydraulic diameter (D$_h$) (mm)	Confinement Ratio (CR)
3	0.0571	0.052
	0.0631	0.0475
	0.0667	0.045
5	0.0571	0.0875
	0.0631	0.080
	0.0667	0.075
7	0.0571	0.122
	0.0631	0.110
	0.0667	0.105
10	0.0571	0.175
	0.0631	0.158
	0.0667	0.150
15	0.0571	0.262
	0.0631	0.237
	0.0667	0.225
20	0.0571	0.350
	0.0631	0.316
	0.0667	0.300

Fig. S1. Loop by loop comparison of particle focusing in zigzag with round corners, asymmetric curvilinear, and zigzag microchannel.
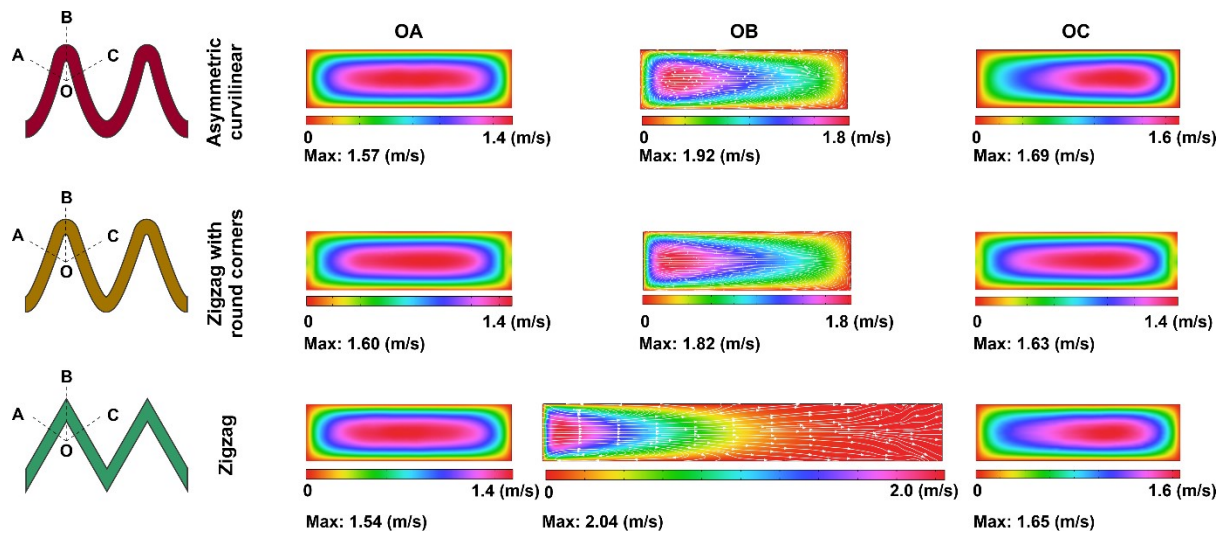
Fig. S2. Numerical analysis of secondary flows at OA, OB, and OC plan in asymmetric curvilinear, zigzag with round corners, and zigzag microchannel. The flow rate was set as 0.3 mL/min. Within the zigzag microchannel, the cross-section expands at the corner; therefore, the Dean forces become stronger and help better in focusing of 3 μm particles that are under the effects of Dean drag forces. Also, increasing the aspect ratio helps maintain the particles at the side walls rather than pushing them through the channel center since particles were affected less by the repulsive force from the long walls. Furthermore, the maximum value of secondary flows at the corners in the zigzag microchannel is more than asymmetric curvilinear and zigzag with round corners. Therefore, the secondary flows become more intensified. These scenarios explain the effects of sharp corners in the zigzag microchannel for better focusing of cells and particles compared to asymmetric curvilinear and zigzag with round corners with the same curvature value.

S1. Numerical Model validation

The DNS model validation was carried out with two different geometries and two different Re.

In Fig. S3A, a trend of nondimensionalized lift force ($C_L = \dfrac{F_L}{\rho(U_M a \kappa)^2}$) at Re=20 and $\kappa = 0.2$ is compared with the trends given by Di Carlo et al. [1] and Martel et al. [2]. As can be seen, uninfluential discrepancies between the results exist. However, a more detailed comparison of lift vectors is also provided for the cross-section as illustrated in Fig. S3B. With that being said, as shown in Fig. S3C, the validation at higher Reynold numbers reveals the preciseness of the current model when compared with the vectors generated by Liu et al. [3] model. Henceforth, it can be concluded that the model calculation follows a similar trend of lift coefficients compared to other references.
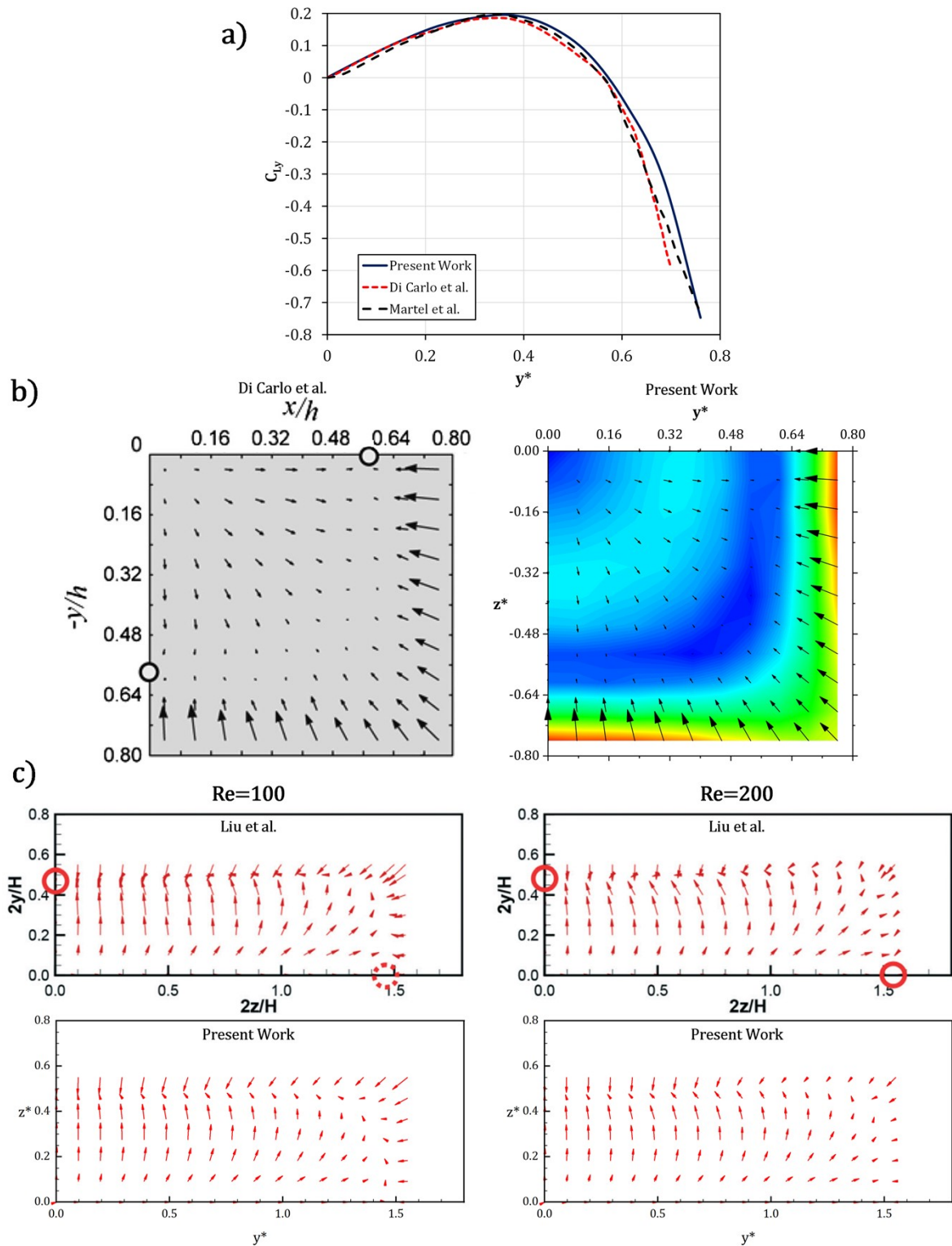
Fig. S3. DNS model validation. a) Quantitative comparison of the lateral lift force between three DNS models including Di Carlo et al. [1] , Martel et al. [2], and the current work. b) Lift force cross-sectional map illustrated by Di Carlo et al. [1] and calculated in the present work shown in the form of vectors. c) Lift distribution and direction comparison between Liu et al. [3] and the present work. The overall comparison of the results at different Reynolds numbers and channel cross-sections implies the validity of the current model. Note that vector length factors are different in each case and similarly the dimensionless sizes.

S2. DNS results

The calculated lift forces which 3 and 15 μm undergo at 300 μL/min in a straight channel are drawn as vector-over-contour in Fig. S4. In the figure, the width and height are nondimensionalized by their corresponding lengths. Bearing in mind the considerable difference in particle size and its reciprocal effect on the surrounding fluid, the lift forces are varied significantly in the middle sector of the cross-section. As a consequence, the larger particle will focus at the locations where the lift force magnitude is relatively small (y*=0 and z*=0.22); however, it is a matter of its path length. Therefore, in a given length of travel inside a periodic channel, when the smaller particles sense insignificant fluid lift, they happen to be dispersed due to the disrupting Dean drag force. The condition for detecting the lift force by a particle is reported empirically to be $Re_p = Re\kappa^2 > 1$ and $\kappa > 0.07$. The rationale behind this inertial focusing/dispersion mechanism is explained by Di Carlo et al. being the balance/imbalance between the magnitude of the decisive forces expressed as [1]:

$$\frac{F_L}{F_D} \sim \frac{1}{\delta} \kappa^3 Re^n \quad (n < 0) \tag{2}$$

where $\delta = \dfrac{H}{2R}$ is curvature ratio with R being the radius of the channel upon which the Dean vortices emerge. The intensity of the secondary flow vortices is determined by Dean number [4]:

$$De = Re\delta^{0.5}. \tag{3}$$

Hence, by decreasing the particle size or increasing Re, the particle exits from the mid-wall focusing state towards the dispersion along the width as a result of the drag dominant flow.
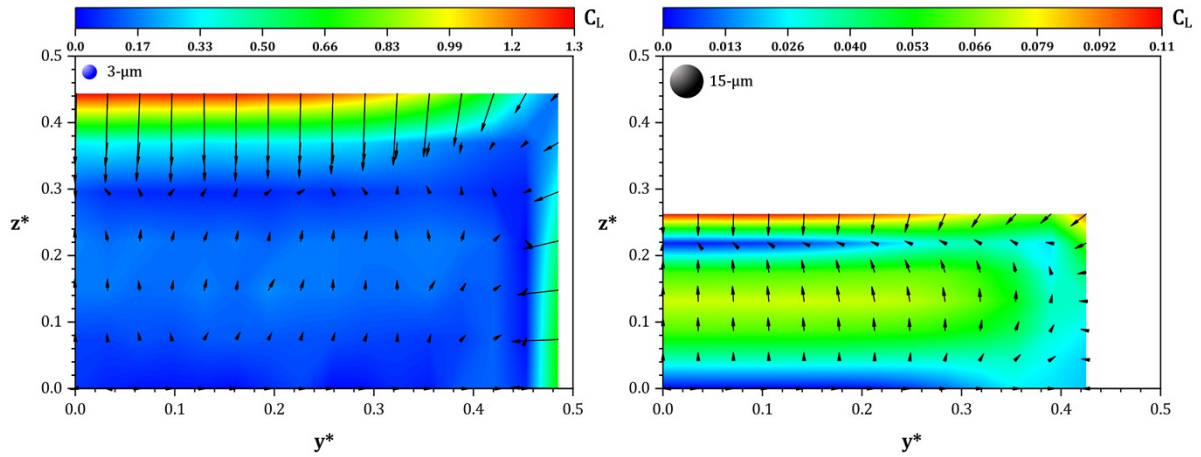
Fig. S4. Vector and contour of lift forces of the studied particles at 300 µL/min. The smaller particle mostly senses a smaller portion of lift in comparison with the larger particle; however, its near-wall repulsion is more dramatic.

Fig. S5 shows the distribution of the nondimensional pressure coefficient, C_p, on the surface of both particles when placed near the channel sidewall. The pressure coefficient is defined as:

$$C_p = \frac{p - p_\infty}{0.5\rho U_M^2}$$

(4)

A pseudo-symmetrical pattern of pressure forms around both particles. However, as the pressure locally increases on the back of the smaller particle, its effective pressure force is more significant than another's. Besides, the 3 µm particle rotates at a higher speed since located at the higher velocity gradient region, and hence, shear stress contributes to the lift force. According to the figure, this contribution must be more predominant for the 15 µm particle as having a larger volume of the surrounding fluid to affect. All in all, the resultant repulsion force is much higher in small particle cases.
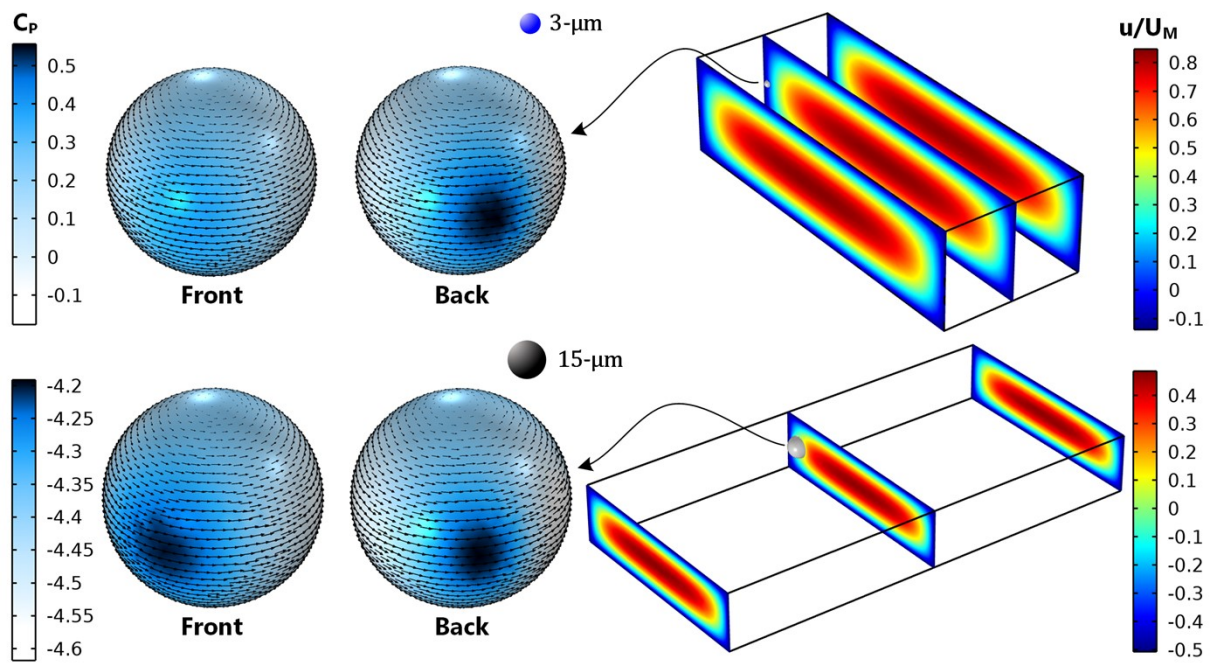
Fig. S5. Pressure coefficient distribution on the particles' surface moving near the wall. Although the particle velocity and size are different, the variation of C_p remains almost periodic along the perimeter of both particles.
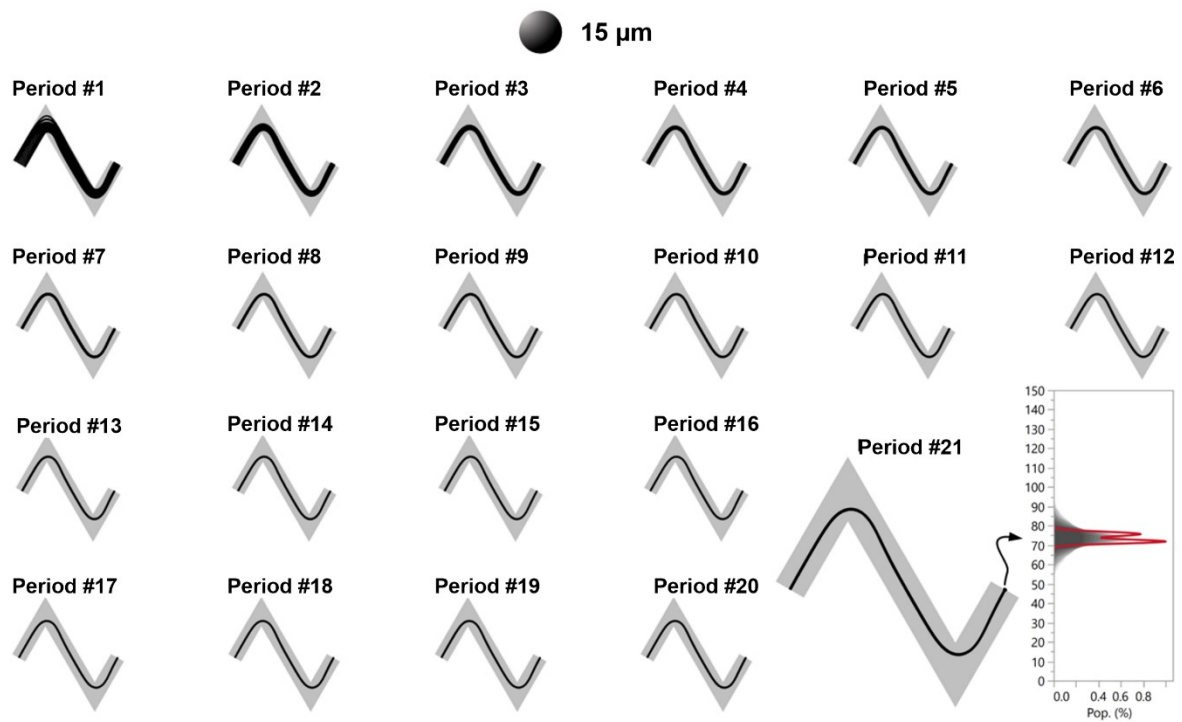
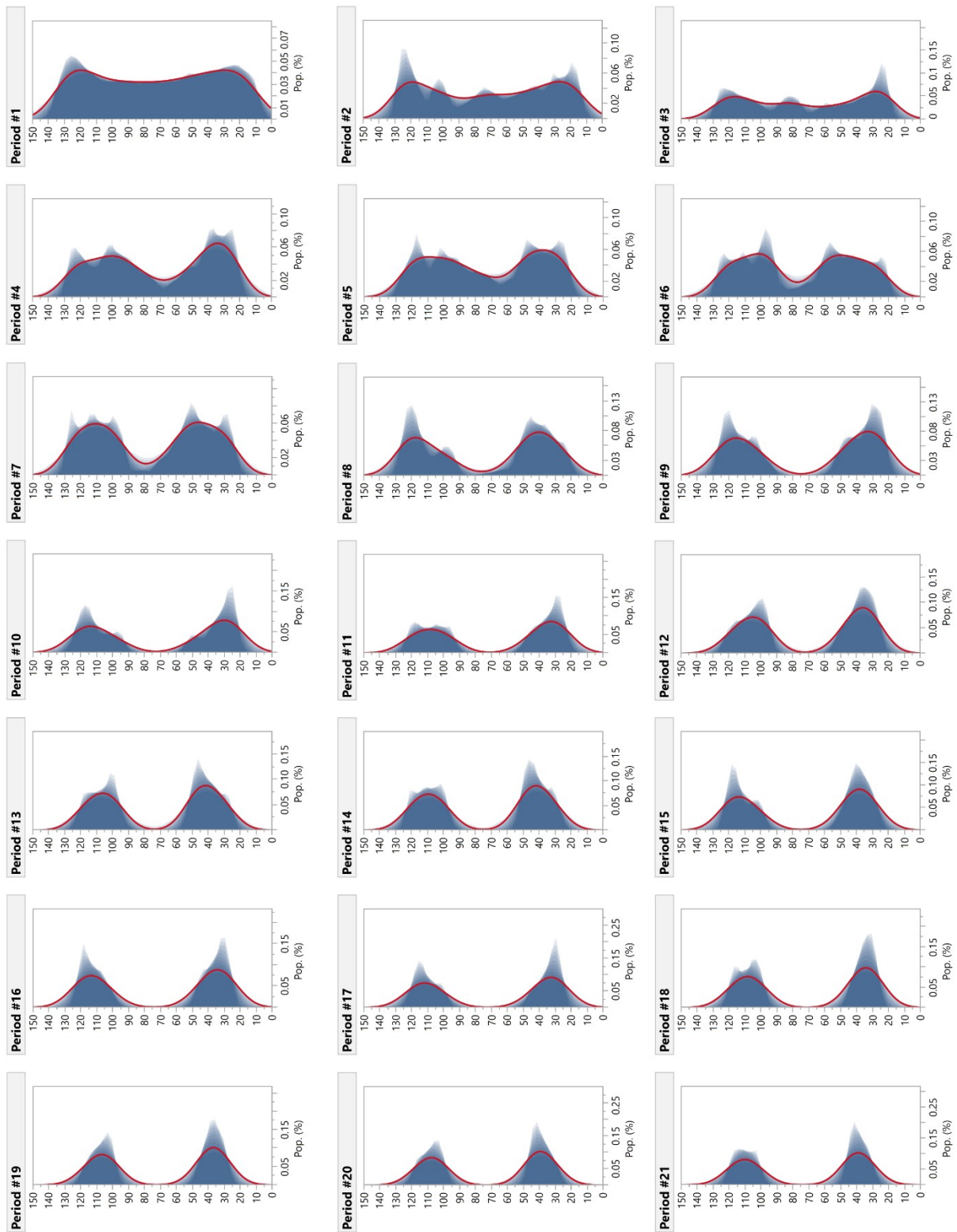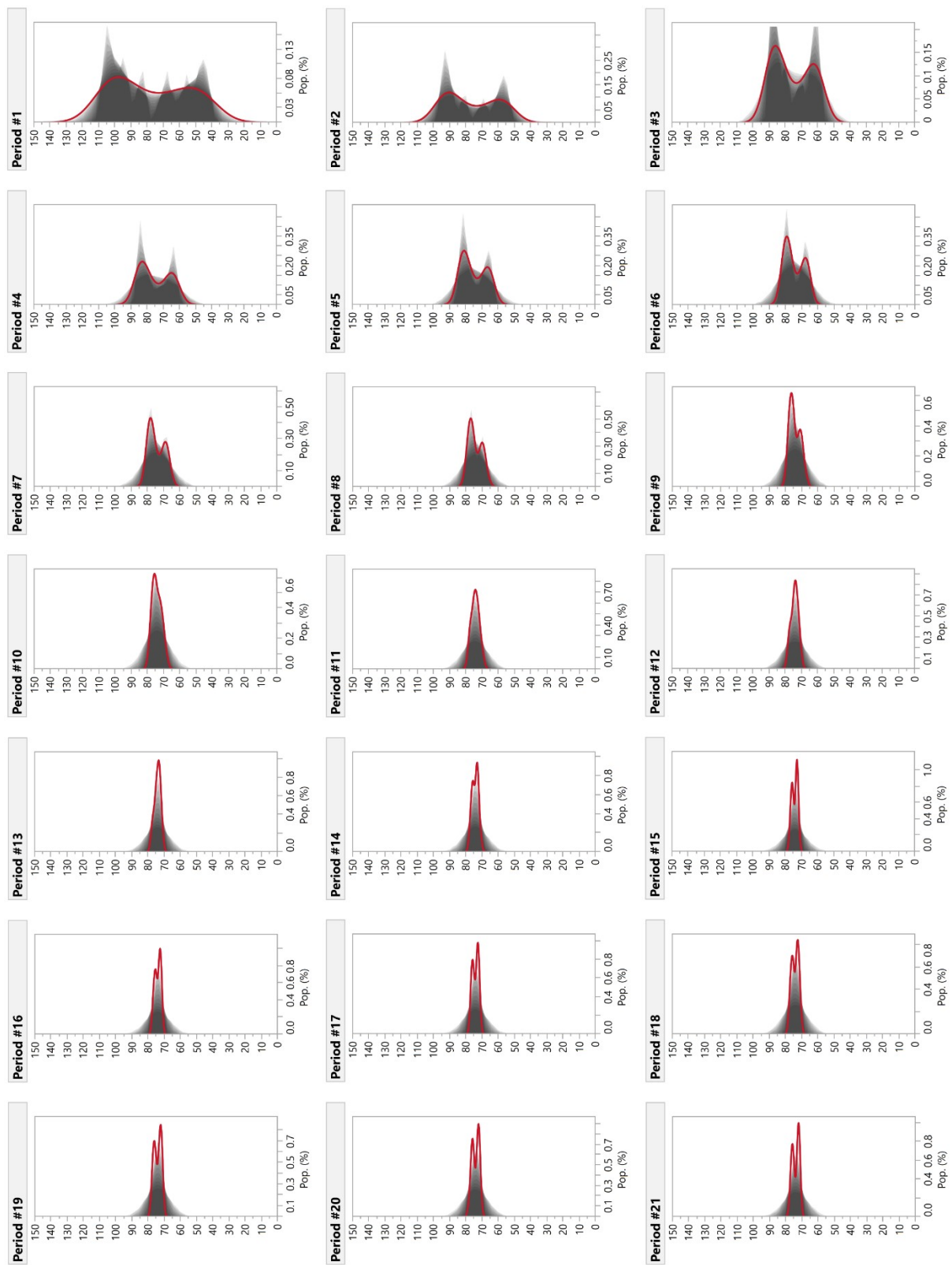**Fig. S6.** Particle trajectory of 15 μm particles across different periods of Z-RISE

Fig. S7. distribution of 3 µm particles across different periods of Z-RISE

Fig. S8. distribution of 15 μm particles across different periods of Z-RISE

S3. Focusing position and focusing length: potential for particle separation

As mentioned earlier, the focusing of particles in zigzag microchannel follows three different focusing patterns, (I) two-sided focusing bands, (II) transition region where there are no specific focusing streams, and (III) single focusing band at the channel center. Here, by examining the transition region II more closely, we observed an interesting phenomenon. In this region, apart from two-sided focusing streams, other distinct focusing streams were observed. As can be seen from Fig. S8, these focusing streams that are expected to be the initial result of the strong wall-induced lift force, due to the stiffness of the channel walls, against shear-induced lift force due to the stiffness of the channel walls, exist before changing the focusing state.

The variations in particle focusing patterns for different channel sizes are shown in Fig. S9. As the particle diameter (^{a}p) increases from 3 μm to 20 μm, several focusing patterns can be observed across the channel width. It can be found that smaller particles were focused along both channel sides and large particles occupied the channel center more compactly. Thus, the possibilities of particle separation exist in zigzag microchannels. Due to the dominant effect of inertial lift force compared to the Dean drag force, a single focusing position along the channel center was achieved. When the flow rates were between the double focusing band and single focusing band, a plus focusing regime was formed.

From Fig. S9A-C, there is a distinct focusing distance between the equilibrium positions of 3 μm particles and other particles at the flow rates from 200 to 400 μl/min exist, which corresponds to the optimal separation condition in this study. At this flow rate, 3 μm particles can be separated from a vast majority of particle sizes from 5 μm to 20 μm particles. The 3 μm particles migrated to the channel sidewalls more slowly than 5 μm and 7 μm particles and were lined up on both sides of the larger particles. When the flow rate continued to increase to 500 μl/min, the large particles were concentrated in a stable focusing state at the almost same

focusing position and small particles remained focused on both channel sides. As channel size increased more, the focusing position of small particles fully overlapped with larger ones where they tend to focus on the channel sides as well. Fig. S9C indicates that the 3 µm and 10 µm particles are located along both channel sides in the double-focusing regime, while the 15 µm particles are ordered in single focusing state at the channel center.

To further investigating the focusing behavior, the focusing length of particles is evaluated (Fig. S9D-F). The focusing length is the required length of the microchannel to fully focus particles on a double or single focusing band. The microchannel short length leads to a reduction in device footprint and fluidic resistance, which will help to overcome the widespread challenges associated with the pressure drop in inertial microfluidic channels. As shown in Fig. S9D-F, the focusing length of particles in all tested microchannels decreased by increasing the flow rate. Small particles tend to focus after a long length (28 mm) and the same focusing length of 27 mm is obtained for flow rates ranged from 200-400 µl/min in the channel size of 57 µm. Compared to Fig. 4, they are lined up in both sides of the microchannel size of 57 µm while their focusing positions overlap at 400 µl/min. Under the same condition, the stable focusing length for 5 µm and 7 µm is observed at 300 µl/min in the channel size of 63 µm. Correspondingly, the slope of the focusing length for all particles changes rapidly in the channel size of 66 µm. The minimum focusing length is achieved at 400 µl/min. Under the same Reynolds number, the large particles (15 µm) are exposed to a greater inertia lift force and are less influenced by the Dean drag force, thus they can achieve focusing position more quickly rather than small particles (3 µm, 5 µm, and 7 µm).
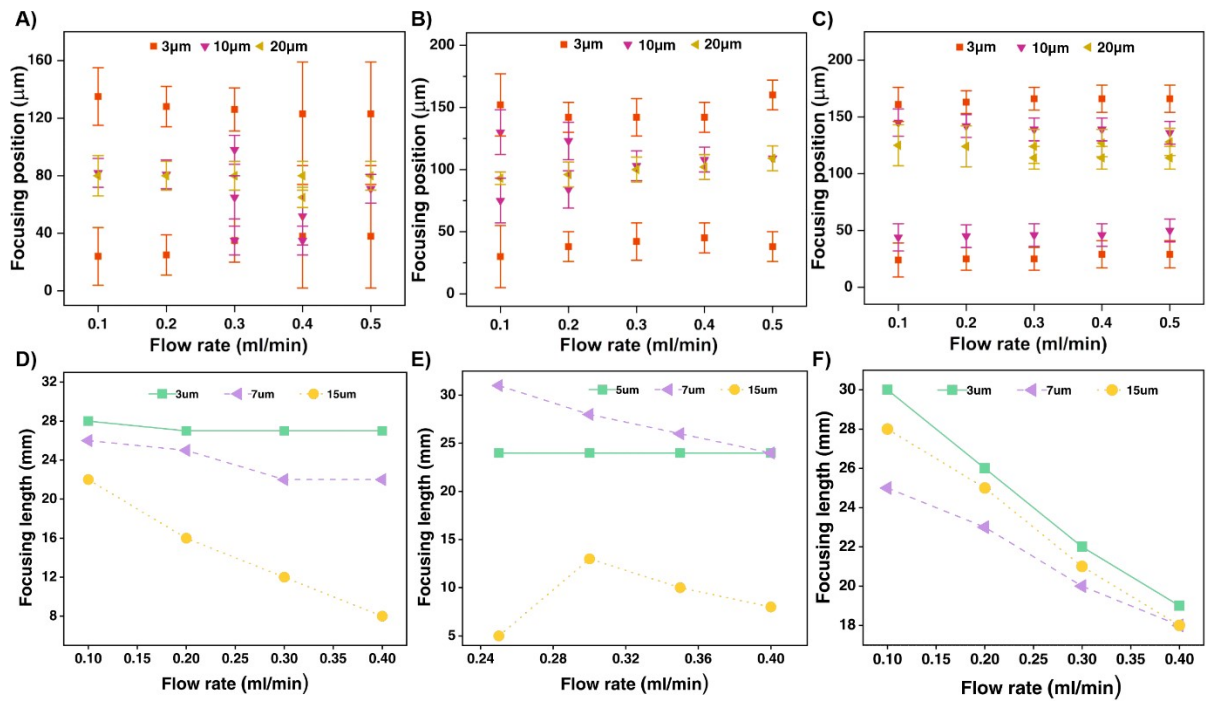
Fig. S9. The focusing position of different particles for various flow rates in the three channel sizes: (A) 57 μm, (B) 63 μm, and (C) 66 μm. The error bars indicate the width of the focusing positions. 3 μm and 10 μm particles were located along both channel sidewalls and 20 μm particles were lined up in the channel centre. There is a distinct distance between the focusing position of 3 μm particles and other particles thereby they can be separated from other particles. All particles were focused in specified streamlines in channel size of 66 μm in flow rates ≥ 200 μm/min. The focusing length of small particles (3 μm, 5 μm, and 7 μm) and large particles (15 μm) in three microchannel sizes (D) 57 μm, (E) 63 μm, and (F) 66 μm. The focusing length is the shortest length to focus particles in a double or single focusing regime. The minimum focusing length is decreased by decreasing the channel size. 3 μm particles achieved stable focusing length in flow rates ≥ 200 μl/min in both channel size of 57 μm and 63 μm. The stable focusing length of 27 mm obtained for 7 μm in the channel size of 57 at flow rate of 300 μl/min. The slope of the focusing length for all particles in the channel size of 66 μm changed rapidly to approximately the same focusing length of 19 μm at 400 μl/min.

Example #S1: Separation of 3 from 10 μm particles

To showcase the ability of the Z-RISE for particle separation, we used a zigzag microchannel with a hydraulic diameter of 62.2 μm and aspect ratio of ~ 0.29 for the separation 3 μm from 10 μm ones. Results show that all 10 μm particles are focused at the channel centerline (Fig. S10A), and all 3 μm particles are focusing at the channel sidewalls (Fig. S10B). The 3 μm outlet does not contain any 10 μm particles (Fig. S10C) since 10 μm particles are big enough to be trapped at the centerline by Dean forces, and due to the superior performance of the zigzag microchannel for sidewall focusing of 3 μm particles, there is not any contamination in 10 μm outlet (Fig. S10D). These results have been confirmed via flow cytometry, showing that the separation and the purity efficiency for both 3 and 10 μm particles are more than 94% (Fig. S10E and F). These results demonstrate the great potential of Z-RISE channels for applied research where high sample purity is of great importance such as the separation of Giardia from fecal samples, platelets from WBCs, or sperm cells from debris and background contaminations.
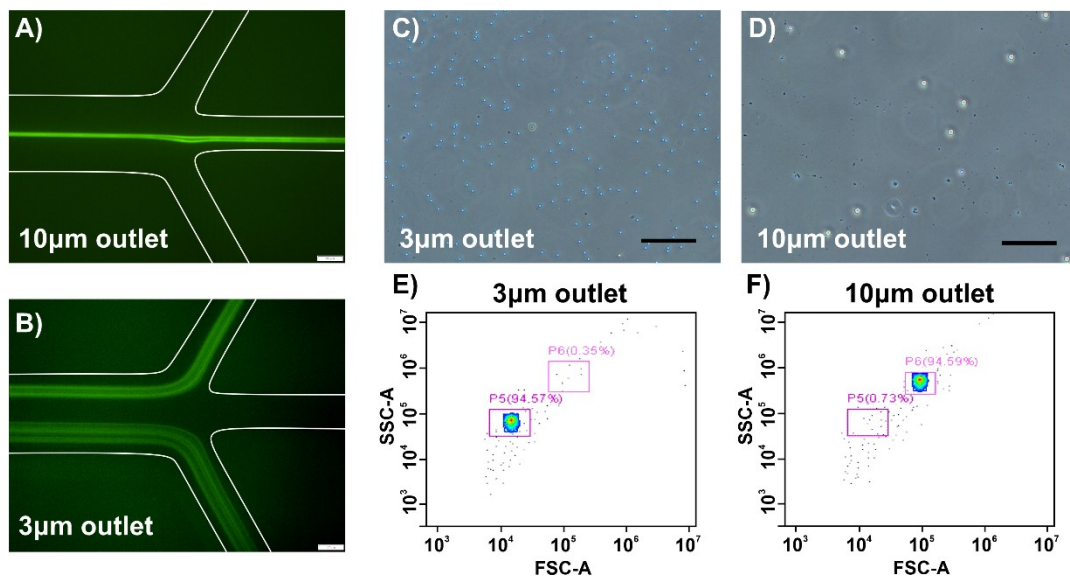
Fig. S10. Case study S1: separating 3 μm from 10 μm particles A) Z-RISE device for particle separation filled with red dye for better channel illustration. B) 10 μm particles are visibly focused at the channel centerline C) where 3 μm particles are focused at the channel sidewalls. The separation purity, as confirmed via flow cytometry is more than 94%, F) outer fraction and G) inner fraction.
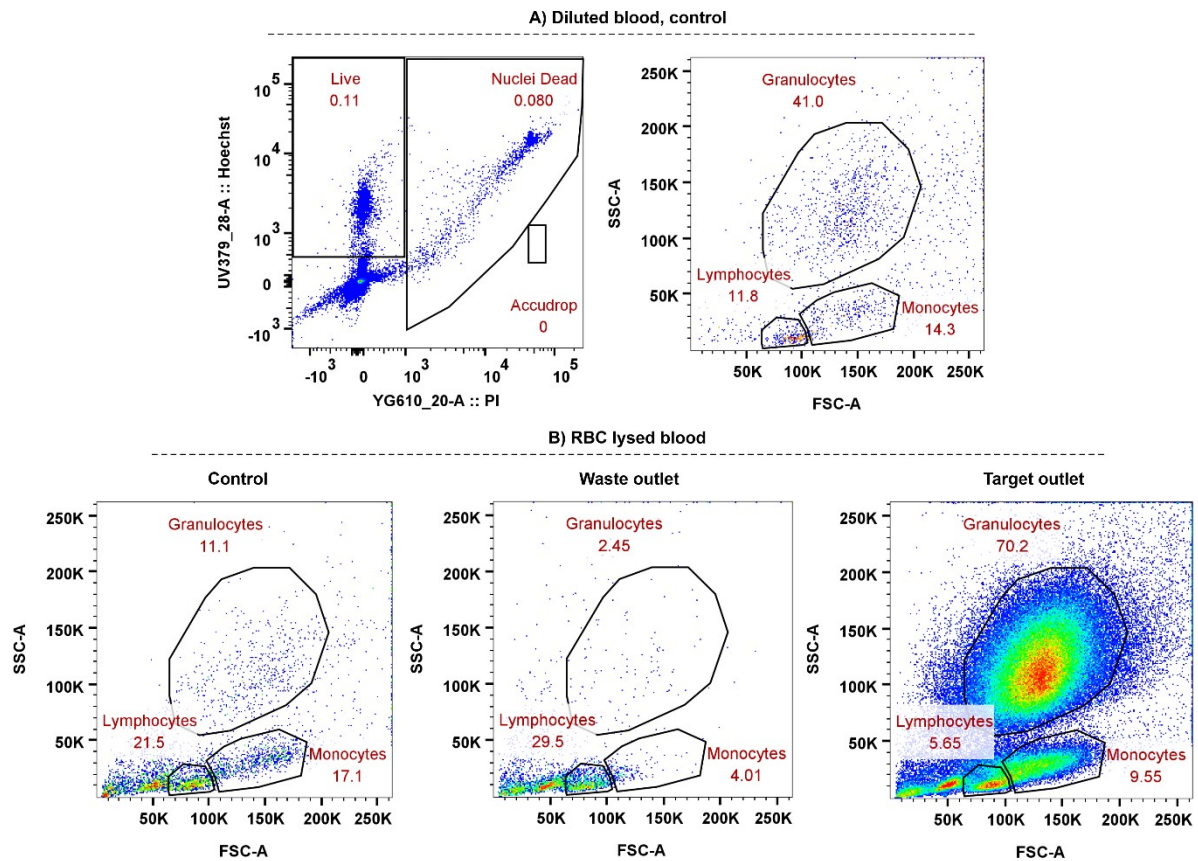
Fig. S11. A) The control sample for the leukocyte subpopulation separation for the diluted blood. For the target outlet, the percentage of live cells to dead cells is ~ 4.01, while for the control sample, the percentage is ~ 1.37. This shows the potential of the Z-RISE microchannel for dead cell and debris removal within the channel while simultaneously enriching leukocyte subpopulations. B) The percentage of lymphocytes, monocytes, and granulocytes in the control sample, waste outlet, and target outlet. The gating has been changed to include all dead and live cells.

References

1.   Di Carlo, D., et al., *Continuous inertial focusing, ordering, and separation of particles in microchannels.* Proceedings of the National Academy of Sciences, 2007. **104**(48): p. 18892-18897.
2.   Martel, J.M., et al., *Continuous Flow Microfluidic Bioparticle Concentrator.* Scientific Reports, 2015. **5**(1): p. 11300.
3.   Liu, C., et al., *A generalized formula for inertial lift on a sphere in microchannels.* Lab on a Chip, 2016. **16**(5): p. 884-892.
4.   Wang, L. and D.S. Dandy, *High-Throughput Inertial Focusing of Micrometer-and Sub-Micrometer-Sized Particles Separation.* Advanced Science, 2017. **4**(10): p. 1700153.